nature communications

Article

https://doi.org/10.1038/s41467-024-54298-8

Yeast metabolism adaptation for efficient terpenoids synthesis via isopentenol utilization

Received: 25 February 2024

Accepted: 6 November 2024

Published online: 13 November 2024

Check for updates

Guangjian Li[1], Hui Liang[1], Ruichen Gao[1], Ling Qin[1], Pei Xu[1], Mingtao Huang[1], Min-Hua Zong[1], Yufei Cao[1,2] & Wen-Yong Lou[1,2]

Microbial biosynthesis has become the leading commercial approach for large-scale production of terpenoids, a valuable class of natural products. Enhancing terpenoid production, however, requires complex modifications on the host organism. Recently, a two-step isopentenol utilization (IU) pathway relying solely on ATP as the cofactor has been proposed as an alternative to the mevalonate (MVA) pathway, streamlining the synthesis of the common terpenoid precursors. Herein, we find that isopentenol inhibits energy metabolism, leading to reduced efficiency of the IU pathway in *Saccharomyces cerevisiae*. To overcome this, we engineer an IU pathway-dependent (IUPD) strain, designed for growth-coupled production. The IUPD strain is compelled to enhance the ATP supply, essential for the IU pathway, and incorporates a high-throughput screening method for enzyme evolution. The refined IU pathway surpasses the MVA pathway in synthesizing complex terpenoids. Our work offers valuable insights into developing growth-coupled strains adapted to efficient natural product synthesis.

Terpenoids, also known as isoprenoids, are abundant natural compounds found in animals, plants, and microorganisms, playing a crucial role in maintaining normal biological activities[1]. These compounds have extensive applications, including use in fragrances, biofuel, colorants, micronutrients, cosmetics, and medicine. However, conventional extraction methods are insufficient to meet the growing market demand for terpenoids[2]. Synthetic biology technology has enabled the design and construction of microbial cell factories, offering a sustainable and scalable solution for terpenoid production. Several valuable terpenoids have been successfully synthesized by engineered microorganisms such as retinol[3], carotenoid[4], ursolic acid[5], and rebaudiosides[6].

The mevalonate (MVA) and methylerythritol 4-phosphate (MEP) pathways represent two classical biosynthetic routes for terpenoids[7], and decades of extensive research have led to substantial advancements in understanding these processes. Despite these accomplishments, the involvement of numerous enzymes and a high demand for cofactors make these two excessively long pathways inherently challenging for terpenoid production. Sophisticated engineering of microorganisms is necessary[8], involving the overexpression of endogenous enzymes and their variants, or introduction of heterologous enzymes, to enhance the supply of precursors[9] and maintain a balance between cell growth and the target production. Recently, the isopentenol utilization (IU) pathway has emerged as a promising alternative synthetic route for terpenoid synthesis[10,11]. The IU pathway is characterized by a two-step conversion from economical bulk chemicals isopentenol to the C_5 precursors of terpenoids, isopentenyl diphosphate (IPP), and dimethylallyl diphosphate (DMAPP)[12], and ATP serves as the only cofactor. This pathway greatly simplifies the challenges in the metabolic engineering of strains.

The IU pathway has been employed to synthesize diverse terpenoids, predominantly in *Escherichia coli*. Pan et al.[13] optimized dehydrogenase expression and fermentation conditions, achieving a

[1]Lab of Applied Biocatalysis, School of Food Science and Engineering, South China University of Technology, No. 381 Wushan Road, Guangzhou, Guangdong, China. [2]Guangdong Province Key Laboratory for Green Processing of Natural Products and Product Safety, South China University of Technology, No. 381 Wushan Road, Guangzhou, Guangdong, China. e-mail: yufeicao@scut.edu.cn; wylou@scut.edu.cn

geranate production of 764 mg/L. Wang et al.[14] enhanced lycopene production to 212.49 mg/L through promoter and ribosome-binding site (RBS) engineering, as well as increasing gene copy number. Zhang et al.[15] achieved 1375.7 mg/L of *cis*-abienol by screening various heterologous phosphatases and knockouting endogenous ones. However, *E. coli* inherently faces limitations in synthesizing complex natural compounds, as their production often necessitates the involvement of glycoproteins, membrane proteins, and other elements. Its lack of post-translational modification systems makes it less effective in protein folding and modification. In contrast, *Saccharomyces cerevisiae*, a widely used eukaryotic model organism, is excellent at synthesizing natural products due to its clear genetic background and feasible genetic manipulation tools. As one of the main production platforms of terpenoids, there have been efforts to incorporate the IU pathway into *S. cerevisiae* for terpenoid synthesis. For instance, Ma et al.[16] increased the geranylgeranyl diphosphate titer through mixed feeding of prenol and isoprenol. However, the impact of introducing the IU pathway and non-natural substrate utilization on the cellular metabolism of *S. cerevisiae* remains unexplored. Engineering *S. cerevisiae* to adapt a non-natural synthetic pathway and enhance the IU pathway efficiency for terpenoid production is important for its application.

In this work, we unveil that isopentenol inhibits the TCA cycle and the cellular respiratory chain in *S. cerevisiae*, leading to inadequate ATP supply and consequently diminishing the IU pathway efficiency. To address this issue, we construct an IU pathway-dependent (IUPD) strain by replacing the MVA pathway with the IU pathway. The growth of IUPD strain is coupled to the IU pathway, compelling cells to enhance ATP production for sustaining growth and reproduction. To further enhance terpenoid production, a high-throughput screening method is developed for enzyme evolution. The engineered IUPD strain shows a 152.95% increase in squalene accumulation. Our work highlights the advantages of a growth-coupling strategy for enhancing terpenoid production in *S. cerevisiae*, offering a platform for enzyme adaptive evolution and demonstrating the construction of growth-coupling properties in other cells.

Results

Rational analysis of IU pathway in *S. cerevisiae*

To explore the impact of IU pathway substrates on *S. cerevisiae*, a transcriptional analysis was performed. Differences in gene expression between two groups, one exposed to isopentenol and the other without, were compared (Fig. 1a). In the presence of isopentenol, cellular energy production and conversion were affected (Fig. 1b). Under aerobic conditions, *S. cerevisiae* converts glucose into ATP through respiration, involving two main processes: (1) substrate-level phosphorylation producing NADH and modest ATP amounts; (2) oxidative phosphorylation of NADH and $FADH_2$ in the inner mitochondrial membrane generating substantial ATP[17,18]. Interestingly, isopentenol was observed to suppress the expression of genes related to the TCA cycle and oxidative phosphorylation, while the expression of genes involved in substrate-level phosphorylation increased (Fig. 1c and Supplementary Fig. 1a). Reporter GO term analysis[19] showed a down-regulation of genes related to the generation of precursor metabolites, energy and cellular respiration (Supplementary Fig. 1b). While *S. cerevisiae* exhibits greater alcohol tolerance than other microorganisms, its growth can be obviously suppressed in the presence of prenol or isoprenol at a concentration of 80 mM[16]. We speculate that isopentenol could induce the dissolution of the lipid components within the cell membrane[20,21], leading to a decline in mitochondrial membrane potential and disruption of oxidative phosphorylation. This leads to reduced ATP production and low IU pathway flux.

Rewiring carbon metabolism through metabolic engineering represents a common strategy to increase ATP supply but involves complex regulation and inherent risks. The MVA pathway is integral to *S. cerevisiae* as terpenoids participate in basic physiological functions of cells, such as electron transfer and maintenance of cell membrane fluidity. We considered whether engineering an IU pathway-dependent (IUPD) strain by replacing *S. cerevisiae*'s MVA pathway with the IU pathway could modulate its metabolic network to enhance ATP supply and maintain growth (Fig. 1d). To test this hypothesis, we initially performed in silico simulations using genome-scale metabolic models[22]. Flux balance analysis (FBA) showed that the strain cannot grow without the MVA pathway (Fig. 1e). Introducing the IU pathway and adding isopentenol restored yeast cell growth; At 0.0186 mmol/g_{DCW}/h, its growth matched the wild-type level. Only a small substrate portion was used for growth recovery, while most were directed into product synthesis. This highlights the IU pathway's higher maximum theoretical yield compared to the MVA pathway.

Substituting the MVA pathway with the IU pathway

FBA reveals that the knockout of *ERG13*, *HMG1/2*, *ERG12*, *ERG8*, or *ERG19* leads to MVA pathway inactivation. *ERG13*, an upstream gene, is an ideal deletion candidate to avoid ineffective carbon conversion. For *S. cerevisiae* with an inactivated MVA pathway, mevalonate is necessary during the growth. PRM10 is predicted to be a pheromone-regulated membrane protein, and the $PRM10^{L156Q}$ facilitates the uptake of mevalonate[23]. Therefore, we introduced $PRM10^{L156Q}$ mutation through the CRISPR/Cas9 system, resulting in the IUP0 strain. After the introduction of $PRM10^{L156Q}$ mutation, the prenol uptake by the IUP0 strain was reduced by 30.88%, whereas isoprenol uptake was unaffected (Supplementary Fig. 2). Subsequently, *ERG13* was knocked out, resulting in the IUP1 strain, which can be rescued by mevalonate supplementation (Supplementary Fig. 3).

The IU pathway converts isopentenol (prenol or isoprenol) into the terpenoid precursors IPP and DMAPP through two-step phosphorylation (Fig. 2a). Choline kinase from *S. cerevisiae* (ScCKI1) and isopentenyl phosphate kinase from *A. thaliana* (AtIPK) are two enzymes commonly used in the IU pathway construction[11,16]. Therefore, the insertion of AtIPK at the *ERG13* site in strain IUP0 led to the substitution of the MVA pathway with the IU pathway, resulting in strain IUP2. Growth comparison between strain IUP1 and IUP2 with varying prenol and isoprenol concentrations (0–20 g/L) showed that strain IUP1, lacking the IU pathway, failed to grow as expected (Supplementary Fig. 4a). In contrast, IUP2 was rescued by prenol (Fig. 2b). Upon the addition of 5 g/L prenol, the OD_{600} value of IUP2 reached 1.12, which was 20.86% of that of wild-type (WT) strain and 26.00% of that of IUP1 cultivated with 20 mM MVA (Fig. 2c). It indicates that prenol can be assimilated into central carbon metabolism, and the IU pathway can function like the MVA pathway, providing C_5 terpenoids precursors for cell growth. The IU pathway, composed of ScCKI1 and AtIPK, has been reported to utilize two isopentenols[13,15,24]. However, supplementation with isoprenol resulted in minimal growth of the IUP2 strain in liquid media. This strain showed only extremely weak growth in spot assays (Supplementary Fig. 4b).

Improving flux of the IU pathway

Although the strain IUP2 can be rescued through prenol supplementation, its growth is inferior to that of the WT strain. This could be attributed to a low IU pathway flux. We attempted to address it by overexpressing ScCKI and AtIPK. Nevertheless, it was unable to improve the strain growth, whether through individual or synergistic overexpression with episomal plasmids in IUP2 (Fig. 3a). This suggested that the key bottleneck is the low enzyme activities. We then evaluated various kinases, including SmDAGK (diacylglycerol kinase form *S. mutans*)[25], MvIPK (IPK from *M. vannielii*)[25], and MtIPK (IPK from *M. tindarius*)[15], to improve the IU pathway. Co-expression of SmDAGK with IPKs greatly enhanced the cell growth with isoprenol supplementation, comparable to the WT, in strains IUP1-4 (SmDAGK with AtIPK), IUP1-5 (SmDAGK with MvIPK) and IUP1-6 (SmDAGK with MtIPK)

https://doi.org/10.1038/s41467-024-54298-8

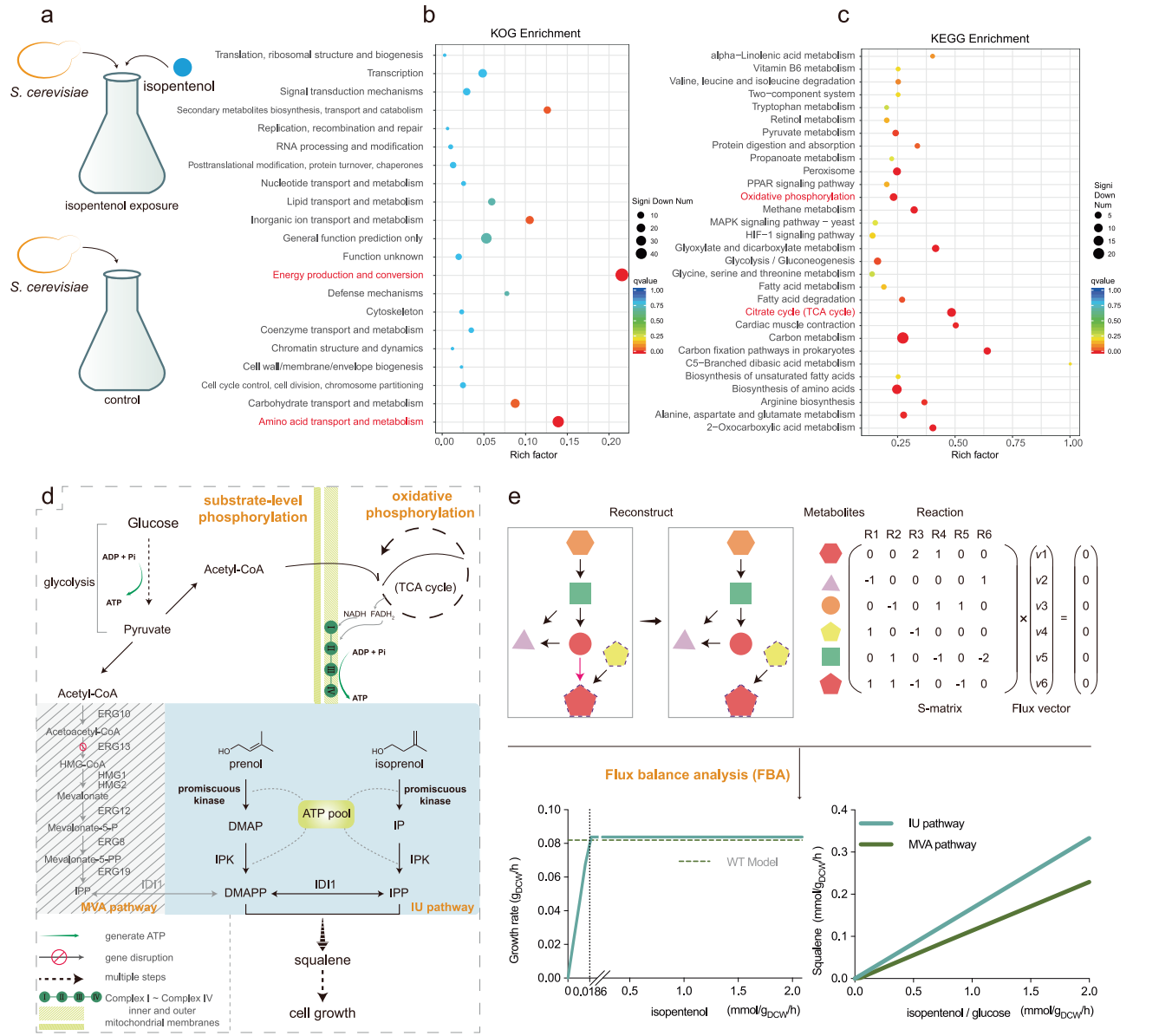

Fig. 1 | Rational analysis of IU pathway in *S. cerevisiae*. **a** Exploring the effect of isopentenol on the metabolism of *S. cerevisiae*. 5 g/L isoprenol was added for co-cultivation with wild-type *S. cerevisiae* (WT + isoprenol group) to assess gene transcriptional levels, compared with the control group without isoprenol (WT group). **b** The scatter plot shows the significant down-regulated physiological activities by KOG enrichment. **c** The scatter plot shows the significant down-regulated biological pathways by KEGG enrichment. **d** Schematic diagram of IUPD strain construction. The IU pathway contains two phosphorylation reactions. Prenol or isoprenol is converted to DMAP (dimethylallyl monophosphate) or IP (isopentenyl monophosphate) subsequently, IPK catalyzes the second phosphorylation reaction to generate DMAPP (dimethylallyl diphosphate) or IPP (isopentenyl diphosphate). The MVA pathway is inactivated by knockout of the *ERG13* gene, and then the IU pathway is introduced. **e** Flux balance analysis. Change the objective to growth when in silico, simulating the effect of different concentrations of isopentenol substrates on IUPD strain growth. Change the objective to squalene synthase, when comparing the maximum theoretical yield of the IU pathway and the MVA pathway. Source data are provided as a Source Data file.

(Fig. 3b). Among these three strains, IUP1-4 showed the highest squalene accumulation (Fig. 3c). Thus, combining SmDAGK and AtIPK effectively restored cell growth and increased squalene accumulation. The strain exhibited poorer growth in the presence of prenol when *AtIPK* was on the plasmid (IUP1-1) rather than integrated into the chromosome (IUP2). This poor cell growth might be attributed to the metabolic burden imposed by the high-copy (2 μ ori) episomal plasmid.

Constructing an IUPD strain demonstrated superiority over directly introducing the IU pathway. Strains with both the MVA and IU pathways (WT-4 and IUP3 in Fig. 3d) moderately increased squalene production through using isoprenol compared to the WT strain. In contrast, the IUPD strains (IUP1-4 and IUP4 in Fig. 3d) showed a 15-fold and 11-fold increase in squalene accumulation. The cell growth of the IUP4 strain reached only 65% of the IUP1-4 strain (Supplementary Fig. 5). We conducted the Real-Time Quantitative PCR (RT-qPCR) analysis to compare the gene expression levels of SmDAGK and AtIPK between IUP3 and IUP4 with isoprenol supplementation (Fig. 3e). Results indicated that the elevated IU pathway flux in IUPD strains is not attributable to changes in the expression levels of the two phosphokinases. To delve deeper into the mechanisms behind the enhanced IU pathways, transcriptional analysis was conducted to gain insight into the regulation and changes of metabolism in IUPD strains. Compared with IUP3 + isoprenol group, IUP4 + isoprenol group exhibited noticeable distinctions in gene transcriptional levels, showing a low correlation between them (Supplementary Fig. 6). In the

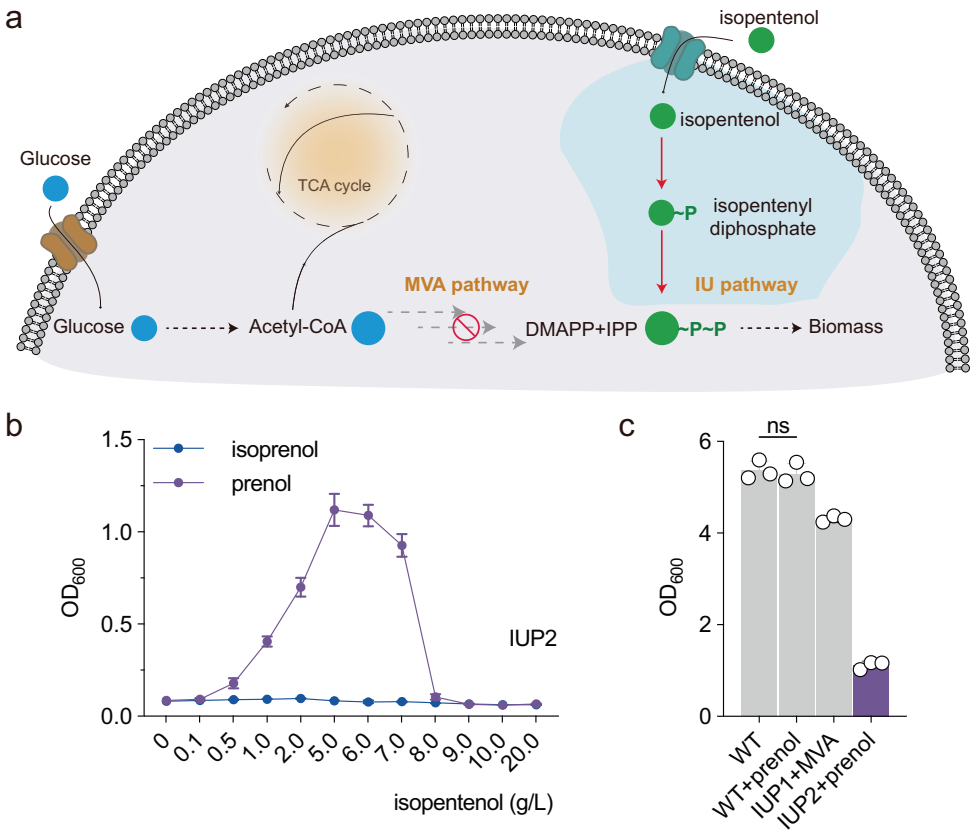

Fig. 2 | Construction of IU pathway-dependent strain. a Schematic diagram of the construction of IUPD strains, substituting the MVA pathway with the IU pathway. **b** Growth of IUP2 in YPD medium supplemented with prenol using 48 deep well plates and isoprenol at various concentrations ranging from 0 to 20 g/L. **c** Comparison of the growth of different strains. Prenol (5 g/L) and MVA (20 mM) were added to the YPD medium as required. Data represent mean value with SD (three independent biological replicates). Statistical significance was evaluated by a two-tailed student's *t* test (ns represents no significant difference, $^{*}p < 0.05$, $^{**}p < 0.01$, $^{***}p < 0.001$). Source data are provided as a Source Data file.

IUP4 + isoprenol group, all glucose transporters except Hxt3, Hxt4, Hxt6 and Hxt7, transcriptional activators of respiratory genes (*HAP1/2/3/4/5*), and part of the TCA cycle genes were up-regulated (Supplementary Fig. 7a and Fig. 3g). This suggests enhanced cellular respiration, ultimately resulting in an increased ATP production (Supplementary Fig. 7b). In addition, the expression levels of three citrate synthases including Cit1, Cit2, and Cit3 increased by 2-fold, 10-fold, and 17-fold, respectively (Supplementary Fig. 7c). Upon *ERG13* knockout, acetyl-CoA ceased to be utilized for terpenoid synthesis. Therefore, the excess acetyl-CoA tends to flow toward the TCA cycle via citrate synthases, subsequently generating a substantial amount of energy (Supplementary Fig. 7d).

Strengthening IU pathway by enzyme engineering

Our earlier findings indicate the crucial role of two phosphokinases in the IU pathway for terpenoid synthesis. We aim to evolve these two enzymes to further enhance the efficiency of the IU pathway. SmDAGK has a homotrimeric structure with 9 transmembrane helices and 3 active sites, which belong to the composite and shared site type[26]. Through molecular docking and enzyme-substrate complex structure analysis, we identified 16 key residues near the active site (Fig. 4a, b, G12, W15, R18, S23, G37, N40, G86, N87, V89, D90, S93, Y95, A101, A102, K105 and A109) and 12 residues near the substrate channel (Fig. 4c, H44, S47, A48, L50, A51, A54, A120, T122, G123, L124, F127 and I131) of SmDAGK. AtIPK is a promiscuous Mg^{2+}-dependent enzyme with a homodimer structure. There are 18 residues near its active site, including K18, A22, K27, H101, R163, T198, S201, G202, D203, P232, S270, A272, D275, T276, T277, G279, M280 and K283 (Fig. 4d, e). The NNK-based codons site saturation mutagenesis was performed to screen for mutants at the mentioned sites with higher catalytic activities.

The IUPD strain, a synthetic auxotroph, serves as an ideal model for high-throughput screening due to its growth-coupled traits[27]. We established a streamlined and efficient high-throughput screening method (all details are provided in Supplementary Fig. 8 and Supplementary Note 1). Briefly, transformed strains were spread on YPD agar plates with 0.5 g/L isoprenol. Most deleterious mutations were naturally eliminated as they failed to support the strain growth. A subset of mutants was further filtered based on their growth (OD_{600} value), and the remaining candidates were subsequently validated through HPLC (Fig. 4f). This method demonstrated accuracy comparable to conventional saturation mutagenesis (Supplementary Fig. 8).

Using our high-throughput screening protocol, saturation mutagenesis libraries of SmDAGK and AtIPK underwent selection, with results presented in Supplementary Fig. 9. Eleven mutants of SmDAGK and eighteen mutants of AtIPK were selected for subsequent validation and combinatorial mutagenesis studies (Fig. 4g). Among the SmDAGK mutants, S47A, S47F, L124A, L124W, S47M, A51L, G123R, and G123F demonstrated increased activity compared to the control. These mutations, located near the cavity, predominantly introduced non-polar residues, enhancing the hydrophobicity of the cavity. $SmDAGK^{S47A,\ L124A}$ represented the most active mutant, with a 77.30% increase in squalene production (Fig. 4g). Specifically, the S47A mutation involved a change from a polar to a non-polar residue, facilitating isoprenol binding, and the L124A mutation reduced steric hindrance by replacing a larger leucine with a smaller alanine

https://doi.org/10.1038/s41467-024-54298-8

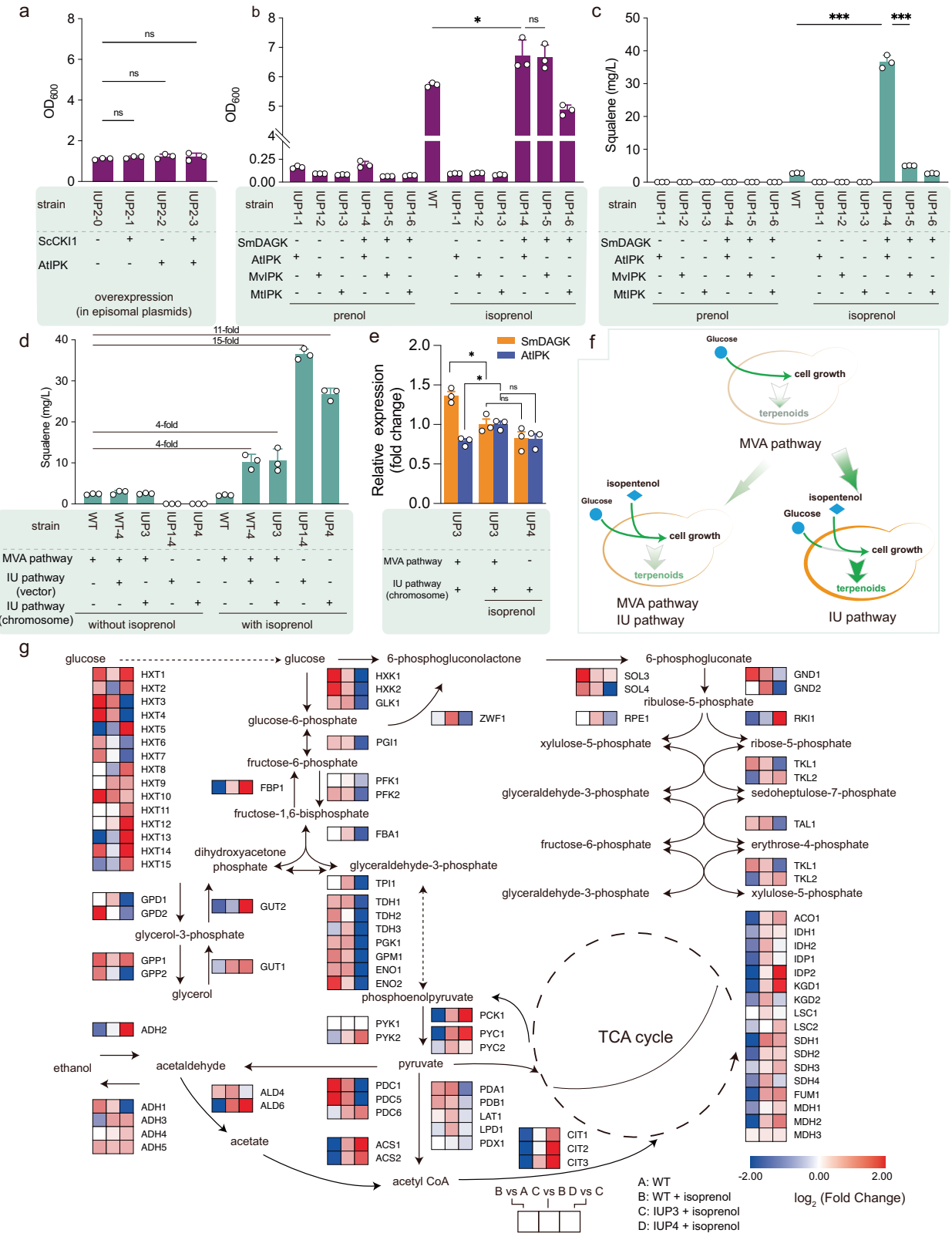

(Supplementary Fig. 10a). SmDAGK$^{S47A, L124A}$ has a larger cavity (Supplementary Fig. 10b), facilitating the entry of bulky ATP. The variant exhibited a higher predicted affinity for isoprenol and ATP compared to its wild-type counterpart near the cavity (Supplementary Fig. 10c). Molecular docking studies indicated that the SmDAGK$^{S47A, L124A}$ altered the microenvironment of the pocket, changing the interacting residues (from H44, S47, S71, G123 to S71, A119, G123 for ATP; from H44, A51, V75, A119 to A48, I72, V75, A119 for isoprenol) and reshaping the binding conformation (Fig. 4h). For AtIPK, 10 mutants, including M280L, P232R, S270P, G279A, G279S, S272R, M280V, S270L, T276M, and P232G, showed higher activity than the wild type (Fig. 4g). The combinatorial mutant AtIPK$^{S270P, A272R}$ displayed the highest activity, showing a 94.88% improvement. The variant has an increased distribution of positive charges near the pocket (Supplementary Fig. 10d)

Fig. 3 | Increasing IU pathway flux to improve cell growth. a Examining the effects of overexpressing ScCKI1 and AtPIK individually or in combination using episomal plasmids, supplemented with 5 g/L prenol. **b**, **c** AtIPK, MvIPK, and MtIPK were expressed individually and synergistically with SmDAGK with episomal plasmids in strain IUP1, supplemented with 5 g/L prenol or isoprenol. $p = 0.04$ between WT and IUP1-4 (isoprenol) compared with OD_{600}. **d** Impact of IU pathway introduction strategy on flux, IU pathway (vector) represents SmDAGK and AtIPK expressed based on episomal plasmids. IU pathway (chromosome) represents SmDAGK and AtIPK expressed based on chromosome integration. The isoprenol concentration was 5 g/L when added. **e** Differences in the expression levels of the SmDAGK gene and AtIPK gene in different strains. $p = 0.0132$ between IUP3 and IUP3 (isoprenol) compared with transcription level of SmDAGK. $p = 0.0110$ between IUP3 and IUP3 (isoprenol) compared with transcription level of AtIPK. **f** Schematic diagram of different IU introduction strategies. Statistical significance was evaluated by a two-tailed student's *t* test (ns represents no significant difference, $^{*}p < 0.05$, $^{**}p < 0.01$, $^{***}p < 0.001$). Data represent mean value with SD (three independent biological replicates). **g** Transcriptional analysis of engineered strains. Four groups included the WT group, WT + isoprenol group, IUP3+isoprenol group, and IUP4 + isoprenol group. Source data are provided as a Source Data file.

and altered loop conformation for ATP binding. Specifically, the Arg272 residue of the variant forms a salt bridge with ATP (Fig. 4i), resulting in a higher ATP binding affinity. The $AtIPK^{S270P,\ A272R}$ mutant also confers a larger catalytic pocket (Supplementary Fig. 10e), which might be beneficial for substrate uptake and phosphorylation. Finally, the synergistic effect of combining $SmDAGK^{S47A,\ L124A}$ with $AtIPK^{S270P,\ A272R}$ led to a 152.95% increase in squalene accumulation.

Advantages of the IUPD strains for terpenoid synthesis

A strengthened MVA (SMVA) pathway (SMVAP1, attained by integrating truncated hydroxymethylglutaryl-CoA reductase (*tHMG1*) and isopentenyl diphosphate isomerase (*IDI1*) to the *GAL80* site of WT strain, Fig. 5a) was compared with the engineered IU pathway (IUP5, created by integrating $SmDAGK^{S47A,\ L124A}$ and $AtIPK^{S270P,\ A272R}$ to *ERG13* site of IUP0, Fig. 5a). By increasing the IUP gene copy number in IUP5, we obtained the IUP6 and IUP7 strains, which greatly enhanced squalene yields to 10.08 and 26.02 mg/g/OD_{600}, representing 4-fold and 10-fold compared to that of SMVAP1 (Fig. 5b). When the engineered IU pathway was integrated with SMVA pathway, the resulting strains SI1 and SI2 produced less squalene and had lower isoprenol conversion rates than their respective IUPD counterparts (strains IUP5 and IUP6) (Fig. 5b, c). The coexistence of both pathways leads to a negative effect on both cell growth and terpenoid synthesis when the isoprenol is supplied (Supplementary Fig. 11). Further analysis showed that the IUP6 strain had higher levels of accumulation of intermediate metabolites, specifically IPP/DMAPP, GPP, and FPP, compared with the SMVAP1 strain (Supplementary Fig. 12).

We further compared the IUPD strategies with the IUP-based yeast systems developed in a previous study[16]. The IUPD strains exhibit an obvious advantage in the production of squalene, limonene, and β-carotene (Fig. 5d–f). Specifically, for squalene and limonene production, the IUPD strains (IUP6 and IUP8) achieved 695-fold and 850-fold increases, respectively, compared to the control strain, surpassing the 11-fold and 16-fold improvements achieved by the previous record strains (PN2 and PN4). For β-carotene production, the IUPD strains (IUP9 and IUP10) showed a 14-fold and 18-fold increase over the control strain, with a 7-fold and 9-fold improvement compared to the SMVA pathway (Fig. 5f).

Discussion

We have demonstrated that IUPD strains hold advantages in the synthesis of various terpenoids. On one hand, the IU pathway simplifies the synthesis process. The production of limonene, squalene, and β-carotene requires only 4, 5, and 8 steps, respectively, compared to 21, 22, and 25 steps in the MVA pathway. On the other hand, the metabolism adaptation to the IU pathway decouples central carbon metabolism from terpenoid synthesis in the IUPD strain, thus enhancing overall efficiency. The synthesis of terpenoids often necessitates additional cofactors. For instance, converting one molecule of phytoene to β-carotene requires four NADPH molecules[28]. Consequently, there may be resource competition between the MVA pathway and later terpenoid synthesis pathways, highlighting the need for intricate regulation to balance the upstream and downstream pathways for enhanced terpenoid production. However, the IU pathway operates orthogonally to heterologous pathways, mitigating resource competition issues. Our engineered IUPD strain can serve as a universal platform for synthesizing terpenoids through simply integrating with efficient downstream pathways.

The IUPD strain consists of both glucose and isopentenol modules. The glucose module supplies reducing power, energy, and essential components such as lipids, while the isopentenol module facilitates efficient terpenoid synthesis. In the glucose module, acetyl-CoA is no longer used for terpenoid synthesis; instead, the redundant acetyl-CoA overflow into other metabolic pathways, leading to the up-regulation of related genes (Supplementary Fig. 7d). Rewiring acetyl-CoA metabolism holds a paramount significance because it can be redirected to enhance the synthesis of ATP, which is essential for terpenoid production. In addition, mitigating the Crabtree effect is crucial for non-ethanol chemical synthesis in *S. cerevisiae*[29,30]. In the isopentenol module, enhancing IU pathway flux, such as increasing the gene copy number, is beneficial for the performance of the IUPD strain.

Our high-throughput screening methods, based on growth-coupled characteristics, reduce the reliance on expensive equipment such as spectral cell sorters and droplet microfluidics systems[31]. Given the essential role of terpenoids as building blocks for cells, the IUPD strain exhibits a robust coupling relationship without the need for intricate calculations or cumbersome metabolic network reprogramming. This coupling relationship enhances the evolutionary robustness of high-yield phenotypes, thereby facilitating global improvements in terpenoid production by IUPD strains through the adaptive evolution of enzymes.

Taken together, this study presents a strategy to develop an IUPD strain by integrating the IU pathway with cell growth, prompting cells to enhance ATP production. The IUPD strains demonstrate a superior potential for terpenoid synthesis through the IU pathway, surpassing strains with both IU and MVA pathways. In addition to limonene, squalene, and β-carotene, the IUPD stains can be utilized to synthesize a wide range of terpenoids (Supplementary Fig. 13). Moreover, DMAPP is the paramount donor for prenylation reactions, and its insufficient supply is the bottleneck in the synthesis of many complex molecules[32]. The IUPD strains also show potential for enhancing the efficiency of the prenylation process. Our work serves as a paradigm for establishing growth-coupled production with IU pathways in other cell platforms.

Methods

Flux balance analysis

The flux balance analysis was based on the consensus *S. cerevisiae* metabolic model Yeast 8.6.2[22] (https://github.com/SysBioChalmers/yeast-GEM/releases/tag/v8.6.2). The COBRA Toolbox 3.0[33] was used for reconstruction and analysis run on MATLAB R2021b (MathWorks, Inc., USA) software. The genes involved in the MVA pathway including *ERG10* (YPL028W), *ERG13* (YML126C), *HMG1/2* (YML075C and YLR450W), *ERG12* (YMR208W) or *ERG8* (YMR220W), *ERG19* (YNR043W) were simulated to be knocked out respectively to obtain the Model_1, Model_2, Model_3, Model_4, Model_5 and Model_6, after which the growth rate of the model was predicted. The code can be found in Supplementary Data 1. For in silico simulation of

https://doi.org/10.1038/s41467-024-54298-8

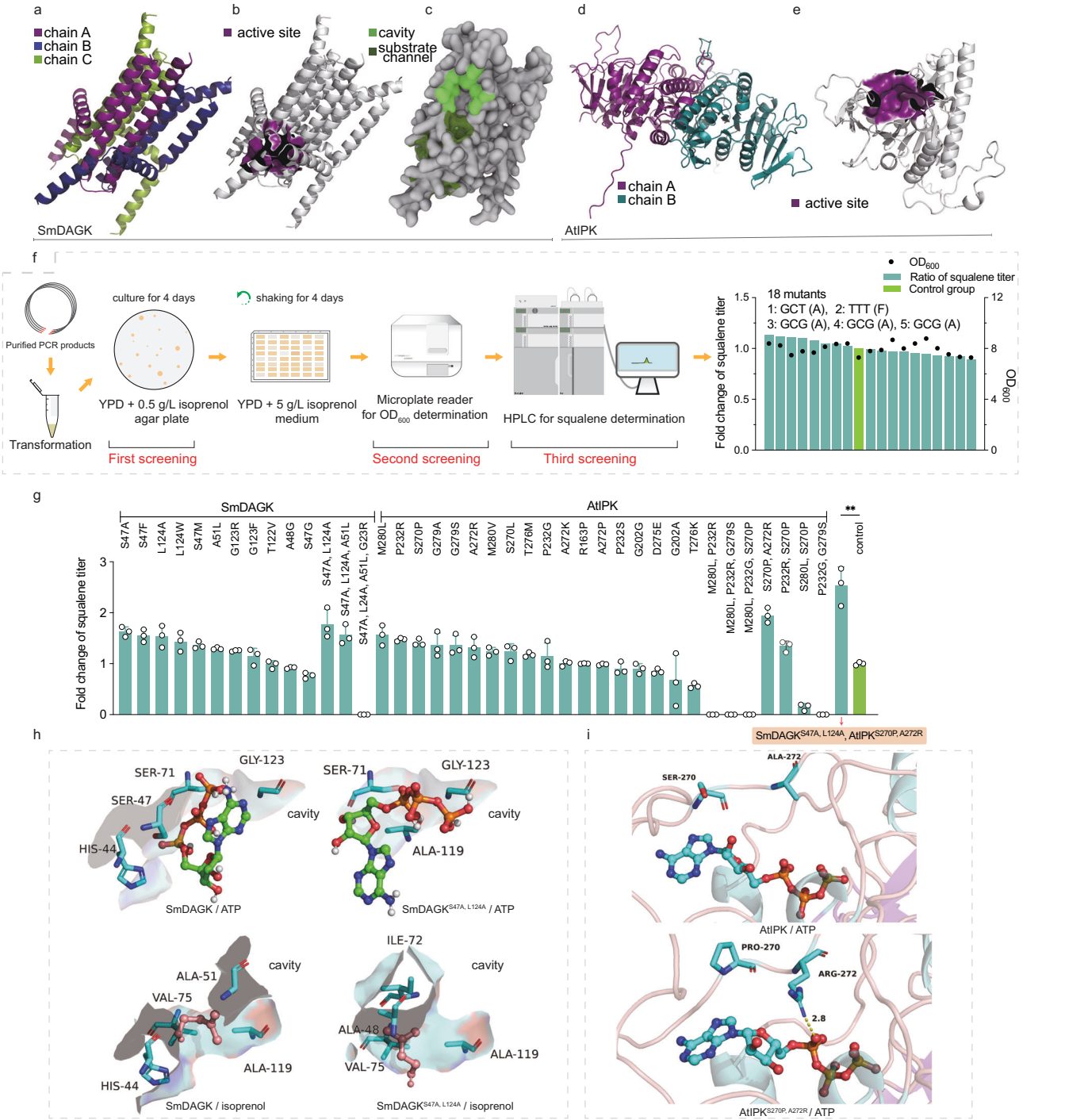

Fig. 4 | Directed evolution of enzymes in IU pathway. a–c Homotrimeric structure of SmDAGK obtained by AlphaFold2, (**b**) shows the active site of SmDAGK, and (**c**) shows the cavity of SmDAGK. **d** Homodimer structure of AtIPK obtained from AlphaFold2. **e** Monomeric structure of AtIPK and its active site. **f** Schematic diagram of high-throughput screening method based on growth-coupled characteristics. **g** Conduct further verification of the promising single-point mutations obtained from SmDAGK and AtIPK, followed by combinatorial mutation. $p = 0.002$ between $SmDAGK^{S47A, L124A}$ + $AtIPK^{S270P, A272R}$ variants and control group compared with squalene titer. Statistical significance was evaluated by a two-tailed student's t test (ns represents no significant difference, $^{*}p < 0.05$, $^{**}p < 0.01$, $^{***}p < 0.001$). Data represent mean value with SD (three independent biological replicates). **h**, **i** Molecular docking results for wild-type enzyme and mutant. The substrate ATP and isoprenol and several key residues were shown. Source data are provided as a Source Data file.

reconstructing IUPD strains, *ERG13* (YML126C) was deleted from original model (model Yeast 8.6.2), metabolites including isopentenol[e], isopentenol[c], isopentenyl monophosphate[c] are created, reactions including isopentenol exchange, isopentenol transport, isopentenol to isopentenyl monophosphate are added. In the original model, the glucose exchange defaults to −1 mmol/g_{DCW}/h, corresponding to the same mass, the isopentenol exchange was set to − 2.09 mmol/g_{DCW}/h. The code can be found in Supplementary Data 2.

Yeast strains and medium

YPD medium consisting of 10 g/L yeast extract (Thermo Scientific™ Oxoid Co., Ltd., USA), 20 g/L peptone (Thermo Scientific™ Oxoid Co.,

https://doi.org/10.1038/s41467-024-54298-8

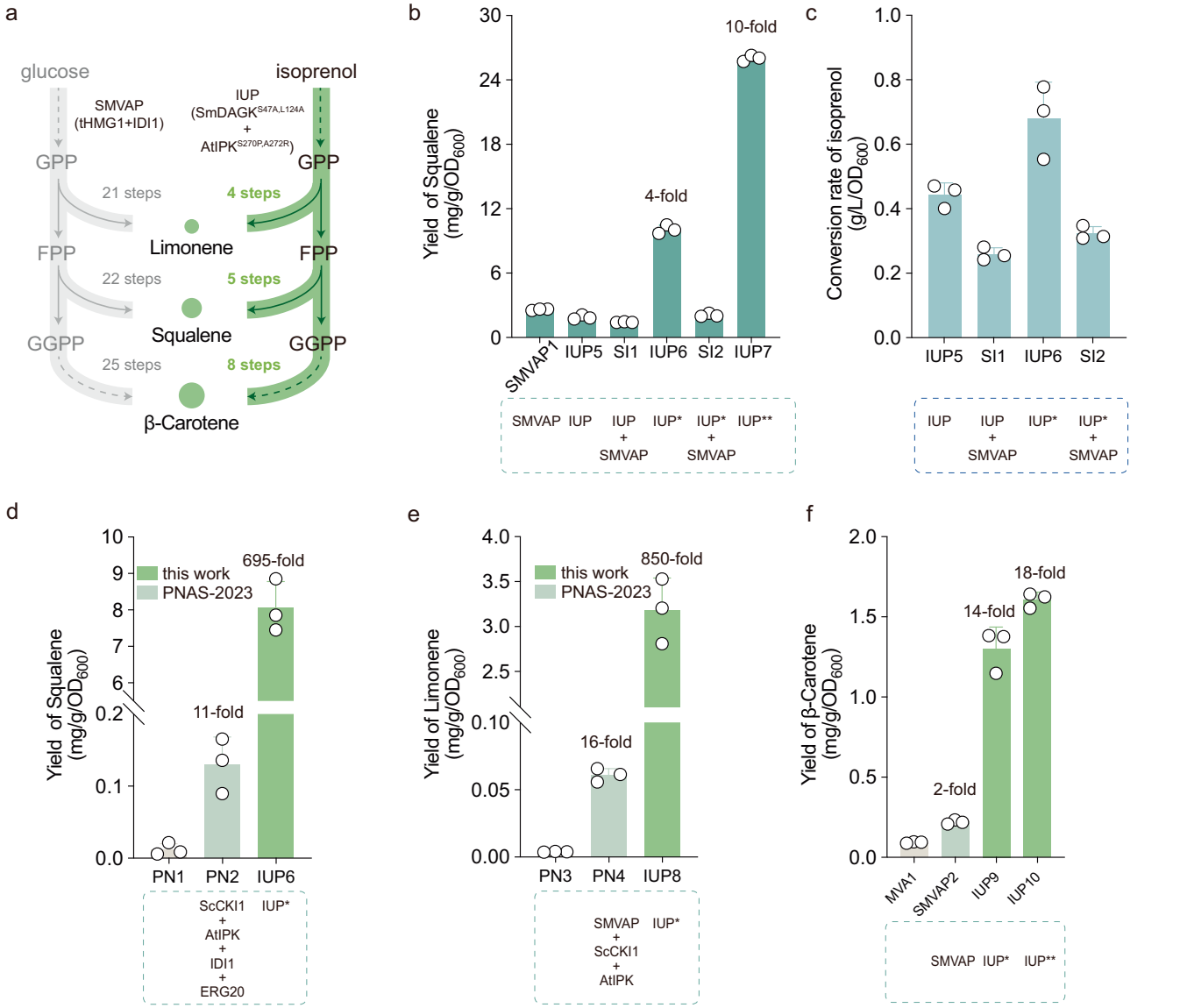

Fig. 5 | Advantages of the IUPD strains for terpenoid synthesis. a Strengthened MVA pathway (SMVAP) obtained by overexpression of tHMG1 and IDI1. IU pathway (IUP) composed of SmDAGK$^{S47A, L124A}$ and AtIPK$^{S270P, A272R}$ variants. **b** The impact of different integration strategies of SMVAP and IUP on squalene yield. IUP* represents 2 copies of IDI1, SmDAGK$^{S47A, L124A}$ and AtIPK$^{S270P, A272R}$ in the yeast chromosome. IUP** represents 3 copies of IDI1, SmDAGK$^{S47A, L124A}$ and AtIPK$^{S270P, A272R}$ in the yeast chromosome. **c** Conversion rates of isoprenol by IUPD and non-IUPD strains. **d** The yield of squalene by different strains. PN1 and PN2 represent strains SCMA00 and SCMA03 used in previous work[16]. **e** The yield of limonene by different strains. The gene of tClLS (encoding truncated geranylgeranyl pyrophosphate synthase from *C. limon*) was used for limonene synthesis. PN3 and PN4 represent strains SCMA10 and SCMA19 used in previous work[16]. **f** The yield of β-carotene by different strains. The synthesis of β-carotene requires the introduction of XdGGPPS (encoding geranylgeranyl pyrophosphate synthase from *X. dendrorhous*), CarB (encoding phytoene dehydrogenase from *M. circinelloides*), and CarRP^{Y27R} (encoding phytoene synthase from *M. circinelloides*). Fermentation was performed in 250 mL shake flasks. Data represent mean value with SD (three independent biological replicates). Source data are provided as a Source Data file.

Ltd., USA) and 20 g/L glucose (Solarbio Life Science Co., Ltd., China) as well as YNB medium consisting of 6.7 g/L yeast nitrogen base without amino acids (Solarbio Life Science Co., Ltd., China), 20 g/L glucose (Solarbio Life Science Co., Ltd., China) for *S. cerevisiae* cultivation. Based on the requirements of the experiment, YNB medium should be supplemented with 50 mg/L histidine, 50 mg/L tryptophan, 50 mg/L leucine (YNB + leu + his + trp), and 50 mg/L uracil (YNB + leu + his + trp + U). In addition, if 5 mM MVA is added, YNB + leu + his + trp + MVA and YNB + leu + his + trp + U + MVA are obtained. The prenol (Aladdin Reagent Co., Ltd., China) and isoprenol (Aladdin Reagent Co., Ltd., China) are filter sterilized with a 0.22 μm sterile syringe filters (Millipore Co., Ltd., USA) before being added to the medium. MVA was prepared by mixing equal volumes of 1 M DL-mevalonolactone (Macklin Co., Ltd., China) aqueous solution and 1 M KOH aqueous solution, then incubating the mixture in a 37 °C water bath for 30 min. After filtration, the MVA solution is stored in the − 20 °C refrigerator.

Plasmid construction

High-fidelity enzyme PrimeSTAR® Max DNA Polymerase (Takara Biomedical Technology Co., Ltd., Japan) was used for polymerase chain reaction (PCR). The PCR Product Purification Kit (Sangon Biotech Co., Ltd., China) was used for purifying DNA fragments, and 2X MultiF Seamless Assembly Mix (ABclonal Technology Co., Ltd., China) was used for plasmid assembly. Subsequently, the assembled plasmids were transformed into *E. coli* DH5α for replication of plasmid. All assembled plasmids were validated through sequencing by Sangon. All genes, including *SmDAGK*, *AtIPK*, *MtIPK*, *MvIPK*, *XdGGPPS*, *CarB*, and *CarRP^{Y27R}*, were codon optimized by the online tool GenSmart

Optimization (GenScript Biotech Co., Ltd., USA) and then synthesized by Sangon. Plasmids p426-P_{TEF1}-SpCas9-T_{CYC1}-P_{SNR52}-PRM10-sgRNA-T_{SUP4}, p426-P_{TEF1}-SpCas9-T_{CYC1}-P_{SNR52}-ERG13-sgRNA-T_{SUP4}, p426-P_{TEF1}-SpCas9-T_{CYC1}-P_{SNR52}-GAL80-sgRNA-T_{SUP4} and p426-P_{TEF1}-SpCas9-T_{CYC1}-P_{SNR52}-CAN1-sgRNA-T_{SUP4} are used for gene editing. All DNA samples are measured for concentration by a K5600C micro-volume spectrophotometer (KAIAO Technology Development Co., Ltd., China).

Genetic modifications

Genetic modifications mainly describe the knockout of the *ERG13* gene, and the editing of other sites is similar. The CRISPR/Cas9 system was employed to introduce the $PRM10^{L156Q}$ mutation in the chromosome. The principle involved selecting the TCATTGGCATTAATCCTGCC sequence as the 20 nt of PRM10's sgRNA (PRM10-sgRNA), which covered the L156 site of *PRM10*. The Cas9 is guided by a designed RNA sequence and binds to a targeted DNA sequence, leading to a double-strand break. Subsequently, under the action of homologous recombination enzymes, achieved homologous recombination between the donor DNA and the chromosome. At the 156th amino acid site of *PRM10* in the recombinant strain, the codon was changed from GAC (leucine) to GTT (glutamine). The Cas9 protein/sgRNA ribonucleoprotein complex, due to a base mutation at the target site, was no longer able to identify and cleave *PRM10*.

The primers PRM10-F and PRM10-R, which have 28 overlapping bases, are used as templates for each other for PCR amplification purified to obtain donor DNA. The Frozen-EZ Yeast Transformation II™ Kit (ZYMO RESEARCH, USA) was used for preparing yeast competent cells. The donor DNA is transformed into the WT yeast strain along with the plasmid of p426-P_{TEF1}-SpCas9-T_{CYC1}-P_{SNR52}-PRM10-sgRNA-T_{SUP4}, then spread onto YNB + leu + his + trp agar plates. After approximately 4-day cultivation at 30 °C in an incubator, the obtained engineered strain (IUP0) was verified for $PRM10^{L156Q}$ mutation through sequencing. The GATTGGTTGACACATTGAGT sequence is the 20 nt of ERG13's sgRNA. The primers ERG13-F and RG13-R that have 18 overlapping bases, are used as templates for each other for PCR amplification purified to obtain donor DNA, which is transformed into the IUP0 along with the plasmid of p426-P_{TEF1}-SpCas9-T_{CYC1}-P_{SNR52}-ERG13-sgRNA-T_{SUP4}, then spread onto YNB + leu + his + trp + MVA agar plate. Single colonies are transferred to YNB + leu + his + trp agar plate for 2-day cultivation. Colonies that fail to grow on YNB + leu + his + trp agar plate are selected from YNB + leu + his + trp + MVA agar plate for further PCR verification. Correct engineered yeast strains were cultivated in YNB + leu + his + trp + U + MVA medium at 220 rpm and 30 °C for 2 days and then spread onto YNB + leu + his + trp + U + MVA with 5-Fluoroorotic acid plates to eliminate the carried plasmid, IUP1 was ultimately obtained. IUP1 had better growth in the YPD-based (YPD supplemented with MVA) liquid medium than in the YNB-based (YNB + leu + his + trp + U + MVA) liquid medium. Interestingly, on the contrary, it hardly grew on the YPD-based agar plate but normally on the YNB-based agar plate (Supplementary Fig. 3). When isolating the single colony is needed, IUP1 should be grown by streaking on YNB + leu + his + trp + U + MVA agar plates (Supplementary Note 2).

The ACGATAGTTGCAGTATGGCG, GACACATTAGTCTCGTATGT, GTAGAAATCAGACGCACGCT, and TTATCCTTAGATATTATACC sequences are the 20 nt of the relevant sgRNAs targeted at *GAL80*, *X-3*, *XI-3* and *CAN1* sites, respectively. The yeast strain construction process is illustrated in Supplementary Fig. 14.

Strain culture

For routine fermentation of *S. cerevisiae* in 48-well plates or 250 mL shake flasks, a single colony is picked and cultured overnight with YPD or YNB medium in a sterile 12 mL culture tube. It is then transferred to YPD medium at an OD of 0.1 and incubated at 220 rpm and 30 °C for 4 days (3 days for β-carotene production). For the production of limonene, 10% (v/v) hexadecane is added. The concentration of isoprenol added to IUP5, IUP6, IUP8 and IUP9 is 5 g/L, and to IUP7 and IUP10 is 2 g/L. The New Cytation 5 Cell Imaging Multi-Mode Reader (BioTek Instruments, USA) is used to determine the OD_{600} value of cells.

Real-time quantitative PCR

For the total RNA extraction of *S. cerevisiae*, 2 mL of exponential phase cells is collected and centrifuged at 15,000 × *g* and 4 °C for 3 min with CF1524R centrifuge (SCILOGEX, USA), and the supernatant is discarded. The cell pellet is washed twice with DEPC-treated water. Then, the cell pellet is mixed with 0.7 g of 0.5 mm glass beads, 300 µL RNA lysis buffer (0.5 M NaCl, 10 mM EDTA, 1% SDS, 0.2 M Tris-HCl pH 7.6), and 250 µL phenol/chloroform/isoamyl alcohol (25:24:1) to 2 mL homogenization tube, and disrupted by high-speed homogenizer for biological samples processing Bioprep-24R (Aosheng Instrument Co., Ltd., China). Then, centrifuge at 4 °C and 15,000 × *g* for 5 min, carefully transfer 200 µL of the upper organic phase to a 1.5 mL centrifuge tube. Add 500 µL of 100% ice-cold ethanol and centrifuge at 4 °C and 15,000 × *g* for 5 min and discard the supernatant. Add 500 µL of 75% ice-cold ethanol to resuspend the RNA, then centrifuge under the same conditions and discard the supernatant. Dry the RNA in a 65 °C metal bath for 10 min to evaporate the water and ethanol. Resuspend in 50 µL DEPC-treated water. The RNA concentration is measured with a micro-volume spectrophotometer. Reverse transcription and genomic DNA degradation are performed using the PrimeScript™ RT reagent Kit with gDNA Eraser (Takara Biomedical Technology Co., Ltd., Japan) and TB Green® Premix Ex Taq™ II (Tli RNaseH Plus) for RT-qPCR. All materials used in the RNA extraction process are RNAse-free to prevent any degradation of RNA samples and ensure the integrity of the results. *ACT1* is used as the housekeeping gene. Primers for *ACT1*, *SmDAGK*, and *AtPK* are ACT1q-F and ACT1q-R, SmDAGKq-F and SmDAGKq-R, AtIPKq-F and AtIPKq-R, respectively.

Transcriptional analysis

The exponential phase cells are collected and centrifuged at 6000 × *g* for 3 min. The supernatant is discarded, and the cells are washed twice with sterile water to obtain the cell pellet. The cells are then flash-frozen in liquid nitrogen and stored at − 80 °C. Transcriptional analysis is conducted by Sangon.

Molecular docking and analysis

Three-dimensional structures of compound ligands (in SDF file format) are downloaded from the PubChem website (https://pubchem.ncbi.nlm.nih.gov). These are converted to PDB file format using OpenBabel 2.4.1 software. AlphaFold2, accessible via a specific Google Colab URL (https://colab.research.google.com/github/sokrypton/ColabFold/blob/main/AlphaFold2.ipynb), is used for predicting and obtaining protein structures. Preprocessing of ligands and enzymes before molecular docking is performed using AutoDockTools 1.5.6. Molecular docking and analysis are conducted using AutoDock Vina. PyMol 2.5.4 is used for visualization. The Protein-Ligand Interaction Profiler[34] (https://plip-tool.biotec.tu-dresden.de/plip-web/plip/index) is used to identify non-covalent interactions between the enzyme and ligand. CavityPlus 2022[35] (http://www.pkumdl.cn:8000/cavityplus) is used for protein cavity detection, and MOLEonline[36] (https://mole.upol.cz) is used for channel analysis.

Transformation protocols for high-throughput screening method

IUP1 is inoculated in 3 mL YPD medium supplemented with 5 mM MVA in a sterile 12 mL culture tube at 30 °C and 220 rpm for 36-48 h. Then, 250 µL of culture is centrifuged at 6000 × *g* for 3 min, discard the

supernatant. The cell pellet is added 100 µL of transformation solution, 1 µg of purified DNA products (Primers for SmDAGK and AtIPK single-point saturation mutations are listed in Supplementary Data 3), and 3 µL of 10 mg/mL ssDNA (Solarbio Life Science Co., Ltd., China). The transformation solution consists of 800 µL PEG3350 (500 g/L), 200 µL LiAc (2 M), and 7.5 µL β-ME, and it can be stored for 6 months at 4 °C. After mixing the cell suspension by a vortex mixer for 10 sec, it is incubated in a 37 °C water bath for 30 min, followed by centrifugation at 6000 × *g* for 3 min, discard the supernatant. The cell pellet is resuspended in 100 µL ddH_2O and spread onto a YPD agar plate supplemented with 0.5 g/L isoprenol, then incubated at 30 °C for 4-5 days. This method is also suitable for routine *S. cerevisiae* plasmid transformation.

We initially tested 188 mutants (from Supplementary Fig. 8 route1-2) and measured their squalene accumulation and OD_{600} values. A Spearman correlation analysis revealed a strong positive correlation between squalene accumulation and OD_{600} values. It indicates that the mutants with increased squalene accumulation generally had OD_{600} values not less than 75% of the WT strain (Supplementary Fig. 8b). Therefore, we used $0.75 \times OD_{600}$ value of the WT strain as the threshold to further screen the mutants (Supplementary Fig. 8 route3).

We performed saturation mutagenesis on 46 sites from two enzymes (SmDAGK and AtIPK). Due to the growth-coupled trait, those strains that exhibit a phenotypically normal appearance on YPD + 0.5 g/L isoprenol plates can be directly selected for fermentation. A total of 385 mutants were selected on plates for fermentation. Based on OD_{600} measurements, we eliminated a subset of 134 mutants. Finally, we used HPLC to determine the squalene accumulation in the remaining 251 mutants. In contrast, the traditional method (each site requires randomly selecting 94 mutants to achieve 95% coverage) would have required measuring the squalene accumulation in 4324 mutants.

Metabolite extraction and analysis

A total of 0.2 mL of fermentation liquid is added to a 2 mL homogenization tube containing 0.7 g of 0.5 mm glass beads and 1 mL of ethyl acetate. The cells are disrupted using Bioprep-24R, followed by centrifugation at 10000 × *g* for 1 min. The upper ethyl acetate layer is then filtered through a 0.22 µm syringe filter for high-performance liquid chromatography (HPLC) analysis, which is conducted using an LC-16 equipped with an SPD-16 dual wavelength UV detector (Shimadzu Corporation, Japan), utilizing an Agilent Poroshell 120 EC-C18 2.1 × 100 mm column (Agilent Technologies Inc., USA). The elution is isocratic with 100% acetonitrile at a flow rate of 0.5 mL/min and a sample volume of 2 µL. Squalene is detected with an elution time of 7.5 min at 210 nm, and β-carotene with an elution time of 15 min at 470 nm. For the determination of limonene, 10 µL of the upper organic layer was added to 990 µL of ethyl acetate, then filtered through a 0.22 µm filter for analysis. Limonene was measured by gas chromatography with an HP-5 column (30 m × 320 µm × 0.25 µm) using Agilent 8890 Gas Chromatograph (Agilent Technologies Inc., USA). The injector temperature was set to 250 °C, and the FID detector temperature was set to 250 °C. The split ratio was 5:1. The column oven temperature was initially held at 80 °C for 3 min, then, increased to 140 °C at a rate of 10 °C per minute, and held for 7 min. Finally, the column oven was heated to 280 °C at a rate of 30 °C per minute and held for 1 min.

To extract intermediate metabolites (IPP/DMAPP, GPP, and FPP), 4 mL of cell culture was centrifuged at 10,000 × *g* for 3 min at 4 °C, and the cell pellet was washed once with ddH_2O. The cell pellet was then disrupted with 0.5 mm glass beads in 0.8 mL of 50% acetonitrile. The mixture was centrifuged at 16,000 × *g* for 10 min at 4 °C. The supernatant was filtered through a 0.22 µm filter. The intermediate metabolites were determined using liquid chromatography-tandem mass spectrometry (LC-MS/MS) comprising a Waters Acquity UPLC (Waters Corporation, USA) and an AB Sciex QTRAP 6500 + System (AB Sciex LLC, USA). An Agilent Poroshell 120 EC-C18 (2.1 × 100 mm) column was utilized, with the mass spectrometry mode set to Multiple Reaction Monitoring (MRM). Solvent A was an aqueous solution of 5 mM NH_4HCO_3, and solvent B was acetonitrile. The gradient elution conditions were as follows: initially, solvent A was at 99% and maintained for 0.5 min. It was then adjusted to 60% at 1.5 min and maintained until 5.5 min. At 7 min, solvent A was adjusted to 1% and maintained until 9 min. At 9.5 min, solvent A was returned to 99% and maintained until 12 min. The flow rate was set to 0.3 mL/min. The isomers IPP and DMAPP could not be separated under these liquid chromatography conditions and were collectively quantified as IPP/DMAPP.

Determination of isopentenol absorption

To determine the absorption rate of isopentenol, yeast was cultured overnight and then inoculated at $OD_{600} = 0.1$ into 250 mL flasks containing 25 mL of YPD medium, followed by incubation for 36 h. The cells were then harvested by centrifugation at 6000 × *g* for 5 min at 4 °C, washed once with 25 mL of sterile 9 g/L NaCl, and resuspended in 25 mL of 9 g/L NaCl. Subsequently, 10 mL of the cell suspension was supplemented with 5 g/L of prenol or isoprenol and incubated at 220 rpm and 30 °C for 12 h with shaking. After incubation, 0.5 mL of the culture was mixed with 1 mL of ethyl acetate, vortexed vigorously for 5 min, and centrifuged at 10,000 × *g* for 3 min. The upper organic layer was then filtered through a 0.22 µm filter for analysis. Isopentenol was measured by gas chromatography. The injector temperature was set to 220 °C, and the FID detector temperature was set to 250 °C. The split ratio was 30:1. The column oven temperature was initially held at 40 °C for 5 min, then increased at a rate of 50 °C per minute to 250 °C, and held for 2 min.

Reporting summary

Further information on research design is available in the Nature Portfolio Reporting Summary linked to this article.

Data availability

Raw data of RNA-seq is deposited in the NCBI BioProject database under accession PRJNA1182314. Primers, genes, plasmids, and strains used in this work are provided in Supplementary Data 3–6. Source data are provided in this paper.

References

1. Bureau, J. A., Oliva, M. E., Dong, Y. & Ignea, C. Engineering yeast for the production of plant terpenoids using synthetic biology approaches. *Nat. Prod. Rep.* **40**, 1822–1848 (2023).
2. Moser, S. & Pichler, H. Identifying and engineering the ideal microbial terpenoid production host. *Appl. Microbiol. Biotechnol.* **103**, 5501–5516 (2019).
3. Park, H. et al. Efficient production of retinol in *Yarrowia lipolytica* by increasing stability using antioxidant and detergent extraction. *Metab. Eng.* **73**, 26–37 (2022).
4. Ma, Y. et al. Removal of lycopene substrate inhibition enables high carotenoid productivity in *Yarrowia lipolytica*. *Nat. Commun.* **13**, 572 (2022).
5. Jin, K. et al. Combinatorial metabolic engineering enables the efficient production of ursolic acid and oleanolic acid in *Saccharomyces cerevisiae*. *Bioresour. Technol.* **374**, 128819 (2023).
6. Xu, Y. et al. De novo biosynthesis of rubusoside and rebaudiosides in engineered yeasts. *Nat. Commun.* **13**, 3040 (2022).
7. Rinaldi, M. A., Ferraz, C. A. & Scrutton, N. S. Alternative metabolic pathways and strategies to high-titre terpenoid production in *Escherichia coli*. *Nat. Prod. Rep.* **39**, 90–118 (2022).

8. Zhu, Z.-T. et al. Metabolic compartmentalization in yeast mitochondria: Burden and solution for squalene overproduction. *Metab. Eng.* **68**, 232–245 (2021).
9. Ye, M., Gao, J. & Zhou, Y. J. Global metabolic rewiring of the non-conventional yeast Ogataea polymorpha for biosynthesis of the sesquiterpenoid β-elemene. *Metab. Eng.* **76**, 225–231 (2023).
10. Clomburg, J. M., Qian, S., Tan, Z., Cheong, S. & Gonzalez, R. The isoprenoid alcohol pathway, a synthetic route for isoprenoid biosynthesis. *Proc. Natl. Acad. Sci. USA* **116**, 12810–12815 (2019).
11. Chatzivasileiou, A. O., Ward, V., Edgar, S. M. & Stephanopoulos, G. Two-step pathway for isoprenoid synthesis. *Proc. Natl. Acad. Sci. USA* **116**, 506–511 (2019).
12. Ward, V. C. A., Chatzivasileiou, A. O. & Stephanopoulos, G. Cell free biosynthesis of isoprenoids from isopentenol. *Biotechnol. Bioeng.* **116**, 3269–3281 (2019).
13. Pan, Q. et al. Biosynthesis of geranate via isopentenol utilization pathway in *Escherichia coli*. *Biotechnol. Bioeng.* **120**, 230–238 (2023).
14. Wang, Y.-Z., Jing, H.-Y., Li, X., Zhang, F. & Sun, X.-M. Rapid construction of *Escherichia coli* chassis with genome multi-position integration of isopentenol utilization pathway for efficient and stable terpenoid accumulation. *Biotechnol. J.* **18**, e2300283 (2023).
15. Zhang, X. et al. Engineering *Escherichia coli* for effective and economic production of cis-abienol by optimizing isopentenol utilization pathway. *J. Clean Prod.* **351**, 131310 (2022).
16. Ma, Y., Zu, Y., Huang, S. & Stephanopoulos, G. Engineering a universal and efficient platform for terpenoid synthesis in yeast. *Proc. Natl. Acad. Sci. USA* **120**, e2207680120 (2023).
17. Lin, Y., Feng, Y., Zheng, L., Zhao, M. & Huang, M. Improved protein production in yeast using cell engineering with genes related to a key factor in the unfolded protein response. *Metab. Eng.* **77**, 152–161 (2023).
18. Yu, T. et al. Metabolic reconfiguration enables synthetic reductive metabolism in yeast. *Nat. Metab.* **4**, 1551–1559 (2022).
19. Varemo, L., Nielsen, J. & Nookaew, I. Enriching the gene set analysis of genome-wide data by incorporating directionality of gene expression and combining statistical hypotheses and methods. *Nucleic Acids Res.* **41**, 4378–4391 (2013).
20. Goldstein, D. B. Effect of alcohol on cellular membranes. *Ann. Emergency Med.* **15**, 1013–1018 (1986).
21. Liu, H. et al. Enhancing biofuels production by engineering the actin cytoskeleton in *Saccharomyces cerevisiae*. *Nat. Commun.* **13**, 1886 (2022).
22. Lu, H. et al. A consensus *S. cerevisiae* metabolic model Yeast8 and its ecosystem for comprehensively probing cellular metabolism. *Nat. Commun.* **10**, 3586 (2019).
23. Kirby, J. et al. Engineering a functional 1-deoxy-D-xylulose 5-phosphate (DXP) pathway in *Saccharomyces cerevisiae*. *Metab. Eng.* **38**, 494–503 (2016).
24. Zhang, Y., Cao, X., Wang, J. & Tang, F. Enhancement of linalool production in *Saccharomyces cerevisiae* by utilizing isopentenol utilization pathway. *Microb. Cell Factories* **21**, 212 (2022).
25. Ma, X. et al. Optimization of the isopentenol utilization pathway for isoprenoid synthesis in *Escherichia coli*. *J. Agric. Food Chem.* **70**, 3512–3520 (2022).
26. Li, D. et al. Crystal structure of the integral membrane diacylglycerol kinase. *Nature* **497**, 521–524 (2013).
27. Chen, J., Wang, Y., Zheng, P. & Sun, J. Engineering synthetic auxotrophs for growth-coupled directed protein evolution. *Trends Biotechnol.* **40**, 773–776 (2022).
28. Li, M., Xia, Q., Zhang, H., Zhang, R. & Yang, J. Metabolic engineering of different microbial hosts for lycopene production. *J. Agric. Food Chem.* **68**, 14104–14122 (2020).
29. Zhang, Y., Su, M., Wang, Z., Nielsen, J. & Liu, Z. Rewiring regulation on respiro-fermentative metabolism relieved Crabtree effects in *Saccharomyces cerevisiae*. *Synth. Syst. Biotechnol.* **7**, 1034–1043 (2022).
30. Dai, Z., Huang, M., Chen, Y., Siewers, V. & Nielsen, J. Global rewiring of cellular metabolism renders *Saccharomyces cerevisiae* Crabtree negative. *Nat. Commun.* **9**, 3059 (2018).
31. Nielsen, J. R., Weusthuis, R. A. & Huang, W. E. Growth-coupled enzyme engineering through manipulation of redox cofactor regeneration. *Biotechnol. Adv.* **63**, 108102 (2023).
32. Yang, S., Chen, R., Cao, X., Wang, G. & Zhou, Y. J. De novo biosynthesis of the hops bioactive flavonoid xanthohumol in yeast. *Nat. Commun.* **1515**, 253 (2024).
33. Heirendt, L. et al. Creation and analysis of biochemical constraint-based models using the COBRA Toolbox v.3.0. *Nat. Protoc.* **14**, 639–702 (2019).
34. Adasme, M. F. et al. PLIP 2021: expanding the scope of the protein–ligand interaction profiler to DNA and RNA. *Nucleic Acids Res.* **49**, W530–W534 (2021).
35. Wang, S., Xie, J., Pei, J. & Lai, L. CavityPlus 2022 update: An integrated platform for comprehensive protein cavity detection and property analyses with user-friendly tools and cavity databases. *J. Mol. Biol.* **435**, 168141 (2023).
36. Pravda, L. et al. MOLEonline: a web-based tool for analyzing channels, tunnels and pores (2018 update). *Nucleic Acids Res.* **46**, W368–W373 (2018).

Acknowledgements

This work was supported by the National Key Research and Development Program of China (2022YFD2101402) to W.L., the National Natural Science Foundation of China (22408113, 22078111, 22108089) to Y.C., W.L. and P.X., the Fundamental Research Funds for the Central Universities (2024ZYGXZR078, 2022ZYGXZR102) to Y.C. and W.L.

Author contributions

G.L. and Y.C. conceived this study. G.L. performed most of the experiments, analyzed the data and drafted the manuscript. H.L. and R.G. participated in molecular docking and analysis of the interaction between enzymes and ligands. L.Q. and M.H. performed the transcriptional analysis. P.X. assisted in the fermentation of yeast. W.L. and M.Z. supervised the project. W.L. and Y.C. contributed to the editing and final approval of the manuscript.

Competing interests

The authors declare no competing interests.

Additional information

Supplementary information The online version contains supplementary material available at https://doi.org/10.1038/s41467-024-54298-8.

Correspondence and requests for materials should be addressed to Yufei Cao or Wen-Yong Lou.

Peer review information *Nature Communications* thanks the anonymous reviewers for their contribution to the peer review of this work. A peer review file is available.